REVIEW

Refractive-index gas thermometry

To cite this article: Patrick M C Rourke *et al* 2019 *Metrologia* **56** 032001

View the article online for updates and enhancements.

Review

Refractive-index gas thermometry

Patrick M C Rourke[1]**, Christof Gaiser**[2]**, Bo Gao**[3]**, Daniele Madonna Ripa**[4]**, Michael R Moldover**[5]**, Laurent Pitre**[6] **and Robin J Underwood**[7]

[1] National Research Council, Ottawa, Ontario K1A 0R6, Canada
[2] Physikalisch-Technische Bundesanstalt (PTB), Abbestrasse 2-12, 10587 Berlin, Germany
[3] Technical Institute of Physics and Chemistry, Chinese Academy of Sciences, Beijing 100190, People's Republic of China
[4] Applied Metrology and Engineering Division, Istituto Nazionale di Ricerca Metrologica (INRiM), 10135 Turin, Italy
[5] Sensor Science Division, National Institute of Standards and Technology, Gaithersburg, MD 20899-8360, United States of America
[6] Laboratoire Commun de Métrologie LNE-Cnam (LCM), 93210 La Plaine Saint-Denis, France
[7] National Physical Laboratory, Teddington, Middlesex TW11 0LW, United Kingdom

E-mail: patrick.rourke@nrc-cnrc.gc.ca

Abstract

The principles and techniques of primary refractive-index gas thermometry (RIGT) are reviewed. Absolute primary RIGT using microwave measurements of helium-filled quasi-spherical resonators has been implemented at the temperatures of the triple points of neon, oxygen, argon and water, with relative standard uncertainties ranging from 9.1×10^{-6} to 3.5×10^{-5}. Researchers are now also using argon-filled cylindrical microwave resonators for RIGT near ambient temperature, with relative standard uncertainties between 3.8×10^{-5} and 4.6×10^{-5}, and conducting relative RIGT measurements on isobars at low temperatures. RIGT at optical frequencies is progressing, and has been used to perform a Boltzmann constant measurement at room temperature with a relative standard uncertainty of 1.2×10^{-5}. Uncertainty budgets from implementations of absolute primary microwave RIGT, relative primary microwave RIGT and absolute primary optical RIGT are provided.

Keywords: thermometry, thermodynamic temperature, refractive index, microwave resonators, polarizability, virial coefficients

(Some figures may appear in colour only in the online journal)

1. Introduction

Refractive-index gas thermometry (RIGT) is the subset of polarizing gas thermometry (PGT) that uses measurements of the refractive index of a gas to determine its density at one or more pressures, and from the density and the pressure, determine the thermodynamic temperature. The physical principles underlying RIGT, as well as the sources of error of the technique, are similar to those of dielectric-constant gas thermometry (DCGT) (Gaiser *et al* 2015), another subset of PGT. However, RIGT is usually realized by measuring the microwave resonance frequencies of gas-filled,

electrically-conducting cavity resonators that have large volume-to-surface-area ratios. Thus, the apparatus is similar to that of acoustic gas thermometry (AGT) (Moldover *et al* 2014) and does not resemble that of capacitor-based DCGT. The microwave resonance frequencies determine the speed of light in the working gas. In contrast, AGT uses the acoustic resonances of similar gas-filled cavities to determine the speed of sound. RIGT microwave resonance measurements, and corrections thereof, are similar to the microwave measurements commonly employed to support AGT (Moldover *et al* 2014). Compared to constant-volume gas thermometry (CVGT), both RIGT and DCGT have the advantage of determining the

density of the gas *in situ* (Gaiser *et al* 2015), with reduced sensitivity to issues of gas sorption, dead volumes and thermomolecular effects that are important in CVGT.

We review the principles and techniques of primary RIGT focusing on the presently-dominant absolute primary RIGT implementations that use microwave resonance measurements to determine the refractive index of helium gas in a quasi-spherical cavity. We also discuss emerging cylindrical cavity RIGT, relative primary RIGT, and optical RIGT approaches. In section 2, we describe the theoretical basis for RIGT including working equations that determine the thermodynamic temperature from experimental measurements of refractive index and pressure. Literature sources of the working gas thermophysical properties needed for the analysis of RIGT data are summarized in section 3, and experimental techniques for refractive index measurement are described in section 4. Section 5 contains a discussion of resonator compressibility, which is the largest component of the uncertainty of current absolute microwave RIGT implementations. Issues related to purity and pressure measurement of the working gas are described in section 6. RIGT uncertainty budgets are given in section 7. Conclusions and anticipated technical improvements are discussed in section 8.

2. RIGT principle

RIGT is based on *in situ* measurement of the density of a gas via measurement of its refractive index n. By combination of the experimental determination of n with independent knowledge of the equation of state of the gas, and measurement of the gas pressure p, the thermodynamic temperature T of the gas is determined.

The refractive index is calculated from the relative dielectric permittivity ε_r and relative magnetic permeability μ_r of a gas using the relation:

$$n = \frac{c_0}{c} = \sqrt{\varepsilon_r \mu_r}, \tag{1}$$

where c_0 is the speed of light in vacuum and c is the speed of light (phase velocity) in the gas. Expansions of ε_r, μ_r, and p as functions of T and the molar gas density ρ are the basis of the RIGT technique:

$$\frac{\varepsilon_r - 1}{\varepsilon_r + 2} = A_\varepsilon \rho \left[1 + b_\varepsilon \rho + c_\varepsilon \rho^2 + \ldots \right] = A_\varepsilon \rho + B_\varepsilon \rho^2 + C_\varepsilon \rho^3 + \ldots, \tag{2}$$

$$\frac{\mu_r - 1}{\mu_r + 2} = A_\mu \rho + \ldots, \tag{3}$$

$$p = RT\rho \left[1 + B_\rho \rho + C_\rho \rho^2 + D_\rho \rho^3 + \ldots \right], \tag{4}$$

where A_ε and A_μ are respectively the molar electric and magnetic polarizabilities of the gas in the limit of zero density, $R = N_A k$ is the molar gas constant (with N_A the Avogadro constant and k the Boltzmann constant), $B_\varepsilon = A_\varepsilon b_\varepsilon$ and $C_\varepsilon = A_\varepsilon c_\varepsilon$ are higher-order dielectric virial coefficients, and B_ρ, C_ρ and D_ρ are higher-order density virial coefficients. Equation (2) is an expression of the Clausius–Mossotti equation, and it

requires the polarizability to be at the same frequency as the refractive index measurement. The microwave frequencies used to measure refractive index in electrically-conducting cavity resonators (typically less than 14 GHz) are effectively static, allowing the static polarizability to be used. For a dilute gas, the above equations may be simplified and combined to produce a low-density, limiting relationship between n, p and T, in the form of the Lorentz–Lorenz equation:

$$\frac{n^2 - 1}{n^2 + 2} = \frac{(A_\varepsilon + A_\mu)\, p}{RT}. \tag{5}$$

Equation (5) may be rearranged and extended to include higher-order virial coefficients by combining equation (4) with an expansion of the refractive index in a similar format to equation (2):

$$\frac{n^2 - 1}{n^2 + 2} = A_R \rho \left[1 + b_R \rho + c_R \rho^2 + \ldots \right], \tag{6}$$

where A_R, b_R and c_R are refractivity virial coefficients, in order to accommodate non-ideal properties of the real working gas (Jousten *et al* 2017):

$$p - \frac{RT}{A_R} \left[\left(\frac{n^2 - 1}{n^2 + 2} \right) + \left(\frac{n^2 - 1}{n^2 + 2} \right)^2 \frac{(B_\rho - b_R)}{A_R} \right.$$
$$\left. + \left(\frac{n^2 - 1}{n^2 + 2} \right)^3 \frac{(C_\rho - 2B_\rho b_R + 2b_R^2 - c_R)}{A_R^2} + \ldots \right] = 0. \tag{7}$$

(A working equation approach to DCGT is similar to equation (7) (Gaiser *et al* 2015).) Based on earlier work establishing the advantages of using quasi-spherical cavity resonators for metrological applications (May *et al* 2004), absolute primary RIGT has been performed at the temperature of the triple point of water with relative standard uncertainty of 9.1 µK K^{-1} (9.1 ppm[8]) (Schmidt *et al* 2007) and at the temperatures of the triple points of neon, oxygen and argon with relative standard uncertainties between 20 µK K^{-1} (20 ppm) and 35 µK K^{-1} (35 ppm) (Rourke 2017). RIGT has also been performed using a cylindrical resonator in the temperature range from 253 K to 303 K with relative standard uncertainties between 38 µK K^{-1} (38 ppm) and 46 µK K^{-1} (46 ppm) (Cui *et al* 2018).

The RIGT measurements of Schmidt *et al* (2007) were analyzed using a virial expansion for n that combines equations (1)–(3) while neglecting small terms:

$$(n^2 - 1)/(3\rho) = (A_\varepsilon + A_\mu) + (A_\varepsilon b_\varepsilon + A_\varepsilon^2)\, \rho$$
$$+ A_\varepsilon \left(A_\varepsilon^2 + 2A_\varepsilon b_\varepsilon + c_\varepsilon \right) \rho^2 + \ldots \tag{8}$$

along with equation (4) relating gas pressures and densities. Note that a factor of 2 missing from the Schmidt *et al* (2007) publication has been restored in equation (8). Equation (8) is equivalent to equation (6), upon which equation (7) is based, with $n^2 + 2 \approx 3$ and

$$A_R = A_\varepsilon + A_\mu, \tag{9}$$

$$A_R b_R = A_\varepsilon b_\varepsilon + A_\varepsilon^2, \tag{10}$$

---

[8] We define 1 part in 10^6 as 1 part per million and abbreviate it as 1 ppm.

$$A_{\mathrm{R}} c_{\mathrm{R}} = A_\varepsilon^3 + 2A_\varepsilon^2 b_\varepsilon + A_\varepsilon c_\varepsilon. \tag{11}$$

Rourke (2017) acquired RIGT data at many (p, T) states. He analyzed his data in two ways. The first analysis (called 'direct (p, T) state evaluation') combined truncated versions of equations (1)–(3), without further approximations:

$$n^2 \approx \left(\frac{1 + 2A_\varepsilon \rho + 2B_\varepsilon \rho^2 + 2C_\varepsilon \rho^3}{1 - A_\varepsilon \rho - B_\varepsilon \rho^2 - C_\varepsilon \rho^3} \right) \left(\frac{1 + 2A_\mu \rho}{1 - A_\mu \rho} \right). \tag{12}$$

He calculated the gas density ρ appearing in equation (12) from the measured p values and trial T values by numerically inverting equation (4), using values of the virial coefficients taken from literature sources. He then determined T for each (p, T) state by finding the trial T value that minimized the difference between the experimentally-measured n^2 and that calculated using equation (12).

In his second analysis, (called 'ideal gas extrapolation') Rourke fitted the (p, n) data on isotherms to polynomial functions of the form:

$$n^2 - 1 = A_n p + B_n p^2 + C_n p^3 + \ldots. \tag{13}$$

The coefficients in equation (13)

$$A_n = \frac{3}{RT} (A_\varepsilon + A_\mu), \tag{14}$$

$$B_n = \frac{3}{R^2 T^2} (A_\varepsilon^2 + B_\varepsilon - A_\varepsilon B_\rho), \tag{15}$$

$$C_n = \frac{3}{R^3 T^3} (A_\varepsilon^3 + 2A_\varepsilon B_\varepsilon + C_\varepsilon - 2A_\varepsilon^2 B_\rho - 2B_\varepsilon B_\rho + 2A_\varepsilon B_\rho^2 - A_\varepsilon C_\rho) \tag{16}$$

were derived by combining equations (4) and (8). Unlike the 'direct (p, T) state evaluation' analysis, the 'ideal gas extrapolation' analysis does not require knowledge of the higher-order virial coefficients beyond A_ε and A_μ, since the coefficients A_n, B_n, C_n, etc are obtained by fitting the experimental data and T is calculated from A_n via equation (14). The thermodynamic temperatures T obtained using both data analyses were mutually consistent within 7 μK K^{-1} (7 ppm) at all three temperatures studied (Rourke 2017).

While the 'ideal gas extrapolation' analysis approach described above does not require independent knowledge of the higher order coefficients B_n, C_n, etc, if *ab initio* estimates of these coefficients are available with useful uncertainties, they may be used to correct the experimental data before fitting. In this way, a third 'hybrid' analysis is in principle possible, whereby T values are determined for each (p, T) state using literature values of the higher virial coefficients in the 'direct (p, T) state evaluation' approach described above, and then fitted as a function of pressure and extrapolated to zero pressure. This approach could allow fitting using a lower-order polynomial than in the pure 'ideal gas extrapolation' analysis, and thus reduce the propagation of uncertainty on the final ideal-gas-extrapolated value of T. Such an approach has not yet been used for analysis of RIGT data: since the overall uncertainty budget of Rourke (2017) is dominated by the uncertainty in the compressibility of the resonator, applying this 'hybrid' approach in place of the 'direct (p, T) state

evaluation' and 'ideal gas extrapolation' analyses would have little effect on the uncertainty in thermodynamic temperature. Nevertheless, this new analysis approach could be valuable when a limited number of pressure points are available and/or a limited pressure range has been explored along the isotherm, particularly when RIGT is performed using gases such as neon or argon, with which 'direct (p, T) state evaluation' is not feasible but sensitivity to the compressibility of the resonator is reduced compared to when using helium.

Gao *et al* (2017) proposed to use RIGT in a relative way and named it single-pressure refractive index gas thermometry (SPRIGT). The microwave resonances are used to determine the refractive index of a working gas in a quasi-spherical resonator at a single pressure. The temperature T can then be determined by comparing the refractive indices measured at T with those measured at a reference temperature T_{ref} (e.g. the triple point of neon). The simplest approximation is based on equation (5) applied at the two temperatures T and T_{ref}, assuming both measurements are made at the same pressure p:

$$\frac{T}{T_{\mathrm{ref}}} = \frac{(n^2(T_{\mathrm{ref}}, p) - 1)}{(n^2(T, p) - 1)} \cdot \frac{(n^2(T, p) + 2)}{(n^2(T_{\mathrm{ref}}, p) + 2)}. \tag{17}$$

Experimental techniques similar to those used for microwave RIGT were used to determine the dimensions of cavity resonators of various shapes (May *et al* 2004, Pitre *et al* 2006, Gavioso *et al* 2011, Pitre *et al* 2011, Underwood *et al* 2011, Feng *et al* 2013, Moldover *et al* 2014, Underwood and Edwards 2014, Gavioso *et al* 2015, Rourke and Hill 2015, Moldover *et al* 2015, Underwood *et al* 2016, Zhang *et al* 2016, Zhang *et al* 2017). The most exacting microwave measurements of dimensions were made to support acoustic gas thermometry. In that context, the average radii of quasi-spherical cavities have been measured with uncertainties below 1 μm m^{-1} (1 ppm) (Pitre *et al* 2011, Underwood *et al* 2011, Gavioso *et al* 2015).

3. Thermophysical properties of the working gas

3.1. Helium

If RIGT is performed in the 'direct (p, T) state evaluation' form (equation (12)), accurate values of the density and dielectric virial coefficients are required. At present this requirement is met only for helium, which has been the focus of detailed *ab initio* calculations. Recent work in this area has resulted in low-uncertainty values of A_ε, both for the static case applicable to microwave RIGT and the dynamic case at optical frequencies (Puchalski *et al* 2016). $A_\mu \equiv 4\pi\chi_0/3$ is obtained from the calculated diamagnetic susceptibility of one helium atom χ_0 (Bruch and Weinhold 2000, 2002, 2003) as treated in Moldover *et al* (2014) and Puchalski *et al* (2016). Because the static A_ε and A_μ are properties of a single atom in its electronic ground state, they are independent of the temperature as long as kT is much smaller than the lowest electronic excitation of the atom. The lowest-lying electronic excitations of helium, neon and argon atoms are all more than 10 eV above their respective ground states (10 eV/$k \approx 1.1 \times 10^5$ K). In

Table 1. Static molar electric and magnetic polarizabilities of helium, neon and argon gases in the limit of zero density. All uncertainties are listed as standard uncertainties.

Property	Value/(cm^3 mol^{-1})	Reference
	Helium	
A_ε	0.517 254 13(6)	Puchalski *et al* (2016)
A_μ	$-0.000 007 921(4)$	Bruch and Weinhold (2000, 2002, 2003)
	Neon	
A_ε	0.994 7114(24)	Gaiser and Fellmuth (2018)
A_μ	$-0.000 0292(6)$	Barter *et al* (1960)
	Argon	
A_ε	4.140 686(10)	Gaiser and Fellmuth (2018)
A_μ	$-0.000 0809(6)$	Barter *et al* (1960)[9]

[9] Average of three literature measurements used by Barter *et al* (1960) to calibrate their instrument.

equilibrium at the temperature T, the excited states have fractional populations on the order of $\exp[-(1.1 \times 10^5 \text{ K})/T]$, so the excited states have negligible effects on the static polarizabilities of these atoms in the temperature range of existing RIGT. The current state-of-the-art literature values of static A_ε and A_μ for helium are listed in table 1.

Quantum statistical values of B_ε calculated by Rizzo *et al* (2002) and earlier quantum statistical calculations by Moszynski *et al* (1995) differ from one another by a roughly temperature-independent offset. The B_ε calculations of Rizzo *et al* and Moszynski *et al*, based on quantum statistical mechanics, have been compared to more recent classical statistical calculations (Cencek *et al* 2011), and the agreement between the results of Rizzo *et al* and Cencek *et al* has been cited as evidence in favour of the quantum statistical B_ε values of Rizzo *et al* over those of Moszynski *et al* (Cencek *et al* 2012, Puchalski *et al* 2016, Rourke 2017). The B_ε discrepancy is likely due to the interaction-induced polarizabilities, which were computed at a substantially higher level by Rizzo *et al* (2002) and Cencek *et al* (2011) than in the earlier work of Moszynski *et al* (1995). Furthermore, because quantum effects on B_ε are small above 77 K (Rizzo *et al* 2002), comparing to the classical calculations of Cencek *et al* (2011) is a good test, since Cencek *et al* used the highest quality potentials and interaction polarizabilities. New quantum statistical calculations would be helpful to ultimately clarify the values of B_ε for helium.

A single classical room temperature estimate of C_ε exists (Heller and Gelbart 1974), though it was published without an estimate of the uncertainty of the calculation. Different authors have taken different approaches to the treatment of the value and uncertainty of C_ε, in all cases ascribing a large uncertainty to it (Schmidt *et al* 2007, Gao *et al* 2017, Rourke 2017). However, in most cases the contribution to the overall uncertainty in T from C_ε is negligible, owing to the relatively low gas densities used in RIGT.

Ab initio calculations of B_ρ (Cencek *et al* 2012) and C_ρ (Garberoglio *et al* 2011) have been confirmed by new calculations using a different theoretical technique (Shaul *et al* 2012), though the uncertainty estimates of the latter work omit the uncertainty of the potential, whereas uncertainty contributions due to the potentials are included with the results of

Cencek *et al* and Garberoglio *et al*. At present, the work of Shaul *et al* (2012) represents the most complete calculation of D_ρ, spanning a temperature range from 2.6 K to 1000 K, though their results at the lowest temperatures may be inaccurate due to the neglect of quantum statistics. The importance of quantum statistics for helium at very low temperature was discussed by Garberoglio and Harvey (2011) in the context of C_ρ calculations.

3.2. Neon and argon

If RIGT is performed in the 'ideal gas extrapolation' form (equations (13)–(16)) or 'hybrid' form, precise knowledge of higher-order virial coefficients is not required, raising the possibility of using working gases other than helium, provided that A_ε and A_μ are known with sufficient accuracy. The current state-of-the-art literature values of A_ε and A_μ for neon and argon are listed in table 1. Recently, Gaiser and Fellmuth (2018) used DCGT to accurately measure A_ε for neon and argon. Since the A_ε values of neon and argon are, respectively, $2\times$ and $8\times$ larger than A_ε of helium, RIGT measurements using neon or argon as a working gas would be less sensitive to uncertainty contributions due to frequency measurements (section 4), resonator compressibility (section 5) and gas purity (section 6). However, neon and argon are subject to significantly larger static pressure head effects than helium (section 6) (Gaiser and Fellmuth 2018). Recent, highly-precise measurements of the refractivity of Ne, Ar, Xe, N$_2$, CO$_2$, and N$_2$O at the optical wavelength $\lambda = 633$ nm are traceable to the calculated refractivity of helium at the same wavelength. This work yields the dynamic molar polarizability of these gases at optical frequencies with a relative standard uncertainty of 1.6×10^{-5}, thereby advancing the prospect of optical RIGT at pressures less than 500 kPa (Egan *et al* 2019).

At present, values of $A_\mu \equiv 4\pi\chi_0/3$ for neon and argon come from χ_0 measurements reported by Barter *et al* (1960). For argon, they used an average of three literature measurements to calibrate their instrument; whereas for neon they directly measured χ_0. However, some theoretical studies have suggested that the absolute magnitudes of the Barter *et al* (1960) χ_0 values for neon and argon may be systematically low by about 7% (Levy and Perdew 1985, Ruud *et al* 1994,

Yoshizawa and Hada 2009), whereas, by comparison, the absolute magnitude of the Barter *et al* (1960) χ_0 value for helium is about 7% higher than that of Bruch and Weinhold (2000, 2002, 2003). Note that a 7% discrepancy in the A_μ values of neon and argon would be comparable in size to the neon and argon A_ε uncertainties of Gaiser and Fellmuth (2018). This situation could be clarified by new *ab initio* magnetic susceptibility calculations for neon and argon with uncertainty of the order of 1%, or by new experimental magnetic susceptibility measurements of neon and argon using an apparatus calibrated with the χ_0 value of helium from Bruch and Weinhold (2000, 2002, 2003).

Unlike helium, the values of the higher density and dielectric virial coefficients of neon and argon are not known accurately enough to enable 'direct (p, T) state evaluation' RIGT analysis. We mention recent experimental and *ab initio* determinations of these coefficients. *Ab initio* calculations of B_ε were performed for neon by Hättig *et al* (2003) and for argon by Vogel *et al* (2010). Experimental measurements of C_ε for both neon and argon are published by Huot and Bose (1991). *Ab initio* calculations of B_ρ and C_ρ for neon were done by both Bich *et al* (2008) and Wiebke *et al* (2012), correcting a typographical error of '$T_0 = 237.15$ K' which should read '$T_0 = 273.15$ K' in the latter reference. For argon, *ab initio* B_ρ values of Mehl are listed in Supplement B of Moldover *et al* (2014), and *ab initio* C_ρ values are found in the publication of Cencek *et al* (2013). *Ab initio* calculations of D_ρ for neon are included in the paper by Wiebke *et al* (2012), correcting the T_0 typographical error as above, and an additional error in which the $t = 2$ coefficient in table 2 of Wiebke *et al* (2012) should read '$-2.677\,80 \times 10^3$' rather than the printed '$-2.677\,80 \times 10^4$'. *Ab initio* values of D_ρ for argon have been published by Wiebke *et al* (2011), correcting a typographical error in which the $t = 6$ coefficient in table 1 should read '$-1.912\,37 \times 10^5$' rather than '$-1.912\,37 \times 10^4$', and in section 3 of the supplementary material of Jäger *et al* (2011). New DCGT measurements at the temperature of the triple point of water by Gaiser and Fellmuth (2019) have verified the theoretical values of B_ρ and C_ρ for neon and argon within the combined standard uncertainties of the experimental and theoretical results.

Argon has been used as a RIGT working gas for the first time by Cui *et al* (2018), who performed thermodynamic temperature measurements between 253 K and 303 K.

4. Refractive index measurement

To date, most RIGT implementations have determined the refractive index by measuring the microwave resonance frequencies of a metal-walled quasi-spherical cavity, initially under vacuum and then again while the cavity was filled with the working gas at a measured pressure (May *et al* 2004, Schmidt *et al* 2007, Rourke 2017). Cylindrical cavity resonators (Underwood and Edwards 2014), which are simpler to construct than those with quasi-spherical cavities, are being used for RIGT (Cui *et al* 2018) and acoustic thermometry applications (Zhang *et al* 2017), including development suited
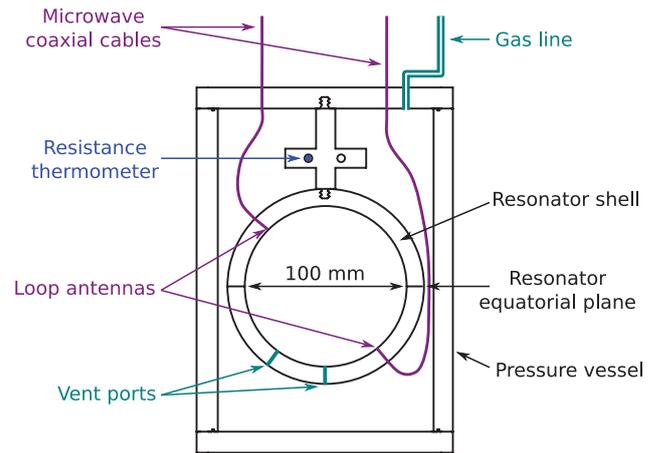
Figure 1. Sketch of the refractive index gas thermometer used by Rourke (2017) between 24.5 K and 84 K.

for demanding high temperature environments (Feng *et al* 2013, Zhang *et al* 2016) where suitable construction materials can be difficult to machine. A sketch of the resonator used by Rourke (2017) is shown in figure 1.

At each temperature T, the refractive index n of gas inside a resonator at pressure p is related to the ratio of the frequencies of a given microwave resonance mode in vacuum, $f_m(0)$, and at pressure p, $f_m(p)$:

$$n = \frac{f_m(0)}{f_m(p)(1 - \kappa_{\text{eff}}p)}. \tag{18}$$

(Here, the subscript 'm' stands for the indices that specify a particular microwave mode.) In equation (18), the term $\kappa_{\text{eff}}\, p$ accounts for the shrinkage of all resonator dimensions under internal and external static gas pressure p. The shrinkage is usually assumed to be isotropic.

Present applications of microwave RIGT combine experimental determinations of the refractive index via equation (18) with either equation (8) (Schmidt *et al* 2007) or equations (12)–(16) (Rourke 2017), as described in section 2 above. In analogy with DCGT, RIGT data may also be analyzed by combining equation (18) with (7) (Gaiser and Fellmuth (2019)):

$$p - \frac{RT}{\left(A_R - \frac{2\kappa_{\text{eff}}RT}{3}\right)} \left\{ \left[\frac{\left(\frac{f_m(0)}{f_m(p)}\right)^2 - 1}{\left(\frac{f_m(0)}{f_m(p)}\right)^2 + 2} \right] \right.$$
$$\left. + \left[\frac{\left(\frac{f_m(0)}{f_m(p)}\right)^2 - 1}{\left(\frac{f_m(0)}{f_m(p)}\right)^2 + 2} \right]^2 \frac{\left(B_\rho - b_R + \frac{2\kappa_{\text{eff}}RT}{3}\left(1 + \frac{B_\rho}{A_R}\right)\right)}{\left(A_R - \frac{2\kappa_{\text{eff}}RT}{3}\right)} + ... \right\} = 0. \tag{19}$$

The ratio of microwave resonance frequencies appearing in equations (18) and (19) can be accurately measured using a microwave vector network analyzer referenced to a frequency standard that is stable during the interval required for thermally-equilibrated measurements of both $f_m(0)$ and $f_m(p)$. (Days, or even weeks may be required to complete an isotherm.) Dimensional stability of the resonator on the same time scale is also important, particularly when measuring at

low pressures using a low-polarizability working gas such as helium, where $f_m(p)$ is close to $f_m(0)$. Simple uncertainty propagation using equations (5) and (18) shows that the contribution of an uncertainty in the microwave frequencies to the relative standard uncertainty in the thermodynamic temperature T scales as $(n^2 - 1)^{-1}$: thus, when measuring at the same temperatures and pressures, using a higher-polarizability working gas such as neon or argon will result in less sensitivity of T to frequency measurement noise, dimensional instabilities and other sources of uncertainty manifested in $f_m(0)$ and $f_m(p)$.

The frequencies of multiple microwave modes are used to determine redundant values of $n(p, T)$. The redundancy is used to assess the influence of unmodelled systematic frequency-measurement errors. For example, Rourke (2017) found that the consistency between the T values obtained using five different microwave modes at 24.5 K was improved by an order of magnitude when using a particular form of the microwave penetration correction (described below), ending up with a standard deviation of the mean over all five modes of approximately 30 μK. Although RIGT has more stringent microwave frequency measurement requirements than typical AGT, the microwave measurements contribute only 10% of the uncertainty of the RIGT temperatures described in Rourke (2017). Yang *et al* (2018) have shown that the microwave signal-to-noise ratio can be improved by using RF amplifiers.

Each microwave resonance mode of a perfectly spherical cavity is composed of $2l + 1$ overlapping peaks, where l is an integer greater than zero. To date, only triplet ($l = 1$) modes have been used for RIGT, as these modes possess the lowest degeneracy. The shapes of quasi-spherical cavities are designed to separate the overlapping triplet peaks into three separate peaks. A convenient choice is a triaxial ellipsoid with a ratio of axis lengths given by $1:(1 + \varepsilon_1):(1 + \varepsilon_2)$ (Mehl *et al* 2004). The dimensionless deformation parameters (ε_1, ε_2) of the cavity used by Schmidt *et al* (2007) were approximately $(1 \times 10^{-3}, 3 \times 10^{-3})$, while those of the cavity used by May *et al* (2004), Rourke and Hill (2015) and Rourke (2017) were approximately $(5 \times 10^{-3}, 1 \times 10^{-3})$. The splitting of the resonance curves into three separate peaks enables the precise measurement of the centre frequency of each peak; relative fitting uncertainties for individual microwave peaks varied from a few parts in 10^{11} to a few parts in 10^9 in the study of Rourke (2017). The average of the three frequencies in a microwave triplet is then nearly equal to the resonance frequency of a perfectly spherical cavity having the same volume as the quasi-spherical resonator, provided that the quasi-spherical shell is smooth (no steps, crevices, holes, etc). Shape-dependent corrections to the measured microwave frequencies have been calculated and applied by Mehl (2009), Edwards and Underwood (2011), Underwood and Edwards (2014), Rourke and Hill (2015) and Mehl (2015). Additional corrections have been applied to account for the presence of vent ports and antennas (Underwood *et al* (2010), Pitre *et al* (2011) and Rourke and Hill (2015)), and for the microwave fields penetrating into the interior surface of the shell (May *et al* 2004, Schmidt *et al* 2007, Rourke and Hill 2015, Rourke 2017). For RIGT, it is important to note that these corrections

are nearly pressure-independent; therefore, they nearly cancel out of the ratio $f_m(0)/f_m(p)$ on each isotherm.

The electromagnetic fields exponentially decay in the shell with a decay ('penetration') length δ that varies as $(\sigma f)^{-1/2}$, where σ is the temperature-dependent electrical conductivity of the shell, and f the mode frequency. Typically, δ ranges from 0.1 μm to 10 μm, depending on the metal comprising the shell. The microwave fields generate electric currents in the decay length in the inner surface of the shell. For each resonance mode, the penetrating fields decrease the resonance frequency f_m by Δf_m and the associated currents increase the resonance half-width g_m. If the inner surface of the metal shell is smooth and isotropic $\Delta f_m = g_m$. Then, one can use the measured values of g_m to correct the resonance frequency for the penetration. However, $\Delta f_m \neq g_m$ is often observed for those modes with induced surface currents that cross the equatorial seam between resonator hemispheres. We also expect $\Delta f_m \neq g_m$ at low temperatures, where the anomalous conductivity effect is important (Inagaki *et al* 1997, Podobedov 2009). On occasion, the inner surface of a shell is plated (e.g. gold plating on a steel shell) to increase its conductivity and to inhibit corrosion. If the plating is less than several penetration layers thick, we expect $\Delta f_m \neq g_m$ (Janney 1957, Tischer 1976). Surface roughness increases both Δf_m and g_m (Tischer 1976, Hernandez *et al* 1986).

Rourke (2017) reported that the mutual consistency among the RIGT temperatures obtained using different microwave modes was greatly improved when he calculated the microwave penetration correction Δf_m using a zero-frequency value of the electrical conductivity at each temperature of interest. He obtained this value from measurements of the widths of resonance peaks with induced surface currents that do not cross the equatorial seam of the quasi-spherical resonator shown in figure 1. Rourke extrapolated the apparent conductivity to zero frequency. His approach circumvented unmodelled, frequency-dependent effects of the seam that increase the measured half-widths. A similar approach, without zero-frequency extrapolation, was employed at room temperature by Underwood *et al* (2011).

Although present RIGT implementations tend to focus on measurements at microwave frequencies, RIGT can also be performed at optical frequencies (Colclough 1974, Rusby 1975). This is an attractive concept because refractive index measurements at moderate gas densities and at optical frequencies have extraordinarily high resolution and because the effects of polar gas impurities are comparatively small at optical frequencies. Progress in this area has been aided by the calculation of the refractive index of helium at optical frequencies with a relative standard uncertainty of 1 ppm at pressures up to 3 MPa (Puchalski *et al* 2016). Recently, Egan *et al* (2016) used an optical interferometer to measure the refractive index of nitrogen in the range 0.1 kPa to 180 kPa at ambient temperature, re-arranging the RIGT equations to determine pressure ratios rather than temperatures. Egan *et al* claim their interferometer realizes the pascal in this range more accurately than competing instruments. While helium dissolves in many optical materials and can change their dimensions in a complicated, time-dependent way, Egan *et al* (2017) have used optical interferometric RIGT with helium at ambient temperature

to measure the Boltzmann constant with a relative standard uncertainty of 12.5 μJ K^{-1}/(J K^{-1}) (12.5 ppm). Thus, refractive index measurements at optical frequencies already have a role in metrology of the thermodynamic states of gases. Laser-based interferometric optical measurement techniques, experimental design and glass construction materials are very different than those used for RIGT measurements in metal resonating cavities at microwave frequencies, and readers are referred to the work of Egan *et al* (2017) and Jousten *et al* (2017) for more details.

5. Resonator compressibility

For absolute primary microwave RIGT, it is crucial to estimate the shrinkage of each dimension of the cavity under the pressure of the working gas. A typical estimate is that each dimension shrinks by the factor $(1 - \kappa_{\text{eff}}\, p)$ where κ_{eff} is the positive compressibility assumed to be $\kappa_T/3$ and where

$$\kappa_T \equiv -\frac{1}{V}\left(\frac{\partial V}{\partial p}\right)_T \qquad (20)$$

is the isothermal volumetric compressibility (inverse of the isothermal bulk modulus) of the shell material. The uncertainty of κ_T is the largest single contributor to the uncertainty of current absolute primary microwave RIGT realizations (Schmidt *et al* 2007, Rourke 2017). As in the case of frequency measurement uncertainty in section 4, simple uncertainty propagation using equations (5) and (18) shows that the contribution of an uncertainty in the shell compressibility to the relative standard uncertainty in the thermodynamic temperature T scales as $(n^2 - 1)^{-1}$: thus, when measuring at the same temperatures and pressures, using a higher-polarizability working gas such as neon or argon will result in less sensitivity of T to the uncertainty in κ_T.

We note that existing realizations of RIGT have used resonators that were assembled from multi-piece shells that were bolted together. For such assembled objects, equation (20) is an approximation that we emphasize by attaching the subscript 'eff' to κ_{eff} in equations (18) and (19). Because the bolts and the shell are made of different materials, the deformation of the assembly under pressure is unlikely to be isotropic. Furthermore, pure polycrystalline cast billets and rolled plates, such as those made from oxygen-free high-conductivity (OFHC) copper, have an anisotropic grain structure that results from metallurgical processing. As a result, a billet or plate may have anisotropic thermal expansions and anisotropic isothermal compressibilities. An additional complication occurs when several parts of a billet and/or plate are assembled into an artifact such as the walls of a cavity. If the assembled object is stress-relieved at one temperature, anisotropic thermal expansions will induce stresses at the joints where different components of the assembly meet. In order to reduce this effect, resonator halves, no matter whether hemispherical or cylindrical, should be machined from the same billet and assembled with a single joint. Typical cylindrical resonators constructed by attaching two ends made from plates to a body made from a billet are not optimized in this

regard. Therefore, in general, the thermal expansion and pressure contraction of the assembled object will not be isotropic and can be only approximately inferred from measurements made on unstressed samples from the same billet or plate.

For application of RIGT at low temperatures, Rourke (2017) used a particular copper resonator that previous measurements had established to be consistent with literature values for the room temperature isothermal compressibility (May *et al* 2004) and temperature-dependent coefficient of thermal expansion (Rourke and Hill 2015) of OFHC copper. Although the isothermal compressibility of copper only increases by about 6% between the triple point of neon and the triple point of water (Simon *et al* 1992, Rourke 2017), the contribution of a temperature-independent uncertainty in the compressibility to the absolute standard uncertainty in the thermodynamic temperature scales like T^2, posing challenges for RIGT measurements at higher temperatures (Rourke 2017).

For application of RIGT at the triple point of water, Schmidt *et al* (2007) used a resonator constructed of maraging steel because this alloy has a low ultrasonic absorption that facilitated the determination of κ_T via resonant ultrasound spectroscopy (RUS) measurements of samples cut from the same billet as the resonator (Schmidt *et al* 2007). RUS can be applied in a straightforward manner using commercial instruments at room temperature; however, extra effort is required to perform RUS at low temperatures (Migliori and Sarrao 1997). Furthermore, as discussed above, samples cut from the same billet will not necessarily have the same compressibility as the assembled resonator artifact. Thus an expedient alternative may be to use RIGT microwave resonance measurements of the cavity at a known thermodynamic temperature (for example, the temperature of the triple point of water) to determine the compressibility of the assembled artifact *in situ*. Then the RUS or RIGT compressibility measurements can be extrapolated to lower temperatures using a method developed by Gaiser and Fellmuth (2016), which is based on the easily-measured thermal expansion and literature values for the specific heat c_p. (c_p of metals is relatively insensitive to processing, except possibly at the very lowest temperatures.) Note that low-temperature RIGT data analyzed using compressibility values extrapolated from higher-temperature *in situ* RIGT measurements would necessarily be considered as relative, not absolute, RIGT.

As pointed out by Schmidt *et al* (2007), in principle there exists an alternative RIGT method that completely circumvents the need to know or determine κ_{eff}. It is a modification of the 'ideal gas extrapolation' analysis that requires microwave resonance measurements to be repeated along isotherms using two different gases, for example, helium and neon. Combining equations (13), (14) and (18), the resonator compressibility term $(1 - \kappa_{\text{eff}}\, p)$ cancels out of the ratio:

$$\left(\frac{f_m^{\text{He}}(p)}{f_m^{\text{Ne}}(p)}\right)^2 = \frac{n_{\text{Ne}}^2(1 - \kappa_{\text{eff}}p)^2}{n_{\text{He}}^2(1 - \kappa_{\text{eff}}p)^2} = \frac{1 + \frac{3\left(A_\varepsilon^{\text{Ne}} + A_\mu^{\text{Ne}}\right)}{RT}p + \cdots}{1 + \frac{3\left(A_\varepsilon^{\text{He}} + A_\mu^{\text{He}}\right)}{RT}p + \cdots}$$

$$= 1 + \frac{3}{RT}\left(A_\varepsilon^{\text{Ne}} + A_\mu^{\text{Ne}} - A_\varepsilon^{\text{He}} - A_\mu^{\text{He}}\right)p + \cdots \cdots$$

$$(21)$$

While this alternative method has the potential to remove the single largest uncertainty component in present absolute primary microwave RIGT implementations, any application thereof comes with several caveats. In addition to doubling the work and time needed to complete a measurement run, the need to repeat measurements with two different gases may cause cross-contamination issues. The successful application of equation (21) requires that the resonating cavity exhibits a low dimensional hysteresis when undergoing cyclic variations of temperature and, to a minor extent, of pressure, though this may be somewhat mitigated by normalizing $f_m^{\text{He}}(p)$ and $f_m^{\text{Ne}}(p)$ by respective vacuum measurements $f_m^{\text{He}}(0)$ and $f_m^{\text{Ne}}(0)$ performed immediately before or after each isotherm. This would have the effect of cancelling out longer-term dimensional instability of the cavity, for example due to thermal cycling. Finally, differing static pressure head corrections for different gases can lead to differences of the pressures inside the resonator even when the pressures measured in the room-temperature gas handling system are the same.

6. Working gas purity and pressure measurement

The choice of helium as the preferred working gas for RIGT is dictated by the superiority of *ab initio* calculations of the thermophysical properties of this gas compared to other gases. However, a significant drawback is that the polarizability of helium is considerably smaller than that of other gases, resulting in a great sensitivity of RIGT to impurities in the working gas. A particularly serious impurity species is water vapour: a polar molecule with a dielectric polarizability (at low frequencies) that is 154 times larger than that of helium near the temperature of the triple point of water. At this temperature, if 1 μmol mol^{-1} amount fraction of water vapour impurity in the helium working gas existed but was undetected and assumed to be zero, the thermodynamic temperature measured by RIGT would be underestimated by 154 μK K^{-1} (154 ppm). While impurities in the helium gas source can be removed by filtering the gas through getters and cold traps, outgassing from the metal walls of gas piping and the resonator itself may be more problematic (de Podesta *et al* 2011). Possible strategies to mitigate the effects of outgassing include flushing with the source gas and baking parts of the gas handling apparatus. The situation is also improved for RIGT experiments performed at low temperatures due to the low vapour pressures of many gas impurity species in that range. Other working gases have higher polarizabilities than helium and are therefore less sensitive to the effects of chemical impurities: for example, the influence of water vapour is 8$\times$ weaker in argon than it is in helium.

Precise control and accurate SI-traceable measurement of the working gas pressure inside the resonator are required for absolute primary RIGT, because the relative standard uncertainty of the pressure realization translates directly to a similarly-sized relative standard uncertainty in the obtained thermodynamic temperature. Typically, this requirement is satisfied by incorporating a calibrated pressure balance into the room-temperature gas handling system supplying the working gas to the RIGT resonator. In order to realize gas

pressure with an uncertainty of a few ppm, great care must be taken with the pressure balance implementation, calibration and corrections, including temperature stability of the balance on the order of 0.2 °C to 0.4 °C (Pavese and Molinar Min Beciet 2013, Zandt *et al* 2015).

Depending on the configuration of the experiment, careful application of a static head correction and thermomolecular correction between the reference plane of the pressure balance and the resonator may be important. Because the static head correction scales with the mass density of the gas, a mistake in this correction would cause a shift in the apparent thermodynamic temperature at all pressures on a given isotherm. The dependence on mass density also means that the static head correction, and its contribution to the relative standard uncertainty of *T*, is more severe at lower temperatures and for heavier working gases than helium (Gaiser and Fellmuth 2018). The uncertainty in the static head correction can be improved by performing intermediate measurements of the gas tube temperature between resonator and pressure balance, particularly in cryostats designed such that thermal gradients are confined to horizontal sections of gas tubing. It is also important, particularly at low temperatures, to repeat measurements using different temperature distributions along the gas tubes to confirm that the static head correction is applied properly; an example is the measurement done at 54 K by Rourke (2017) using a different cryocooler stage 1 set point than used for the other 54 K isotherms in that work.

The thermomolecular correction can be minimized by ensuring the gas tube diameter is much larger than the molecular mean-free path (Pavese and Molinar Min Beciet 2013, Fellmuth *et al* 2018, Steur *et al* 2018). In connection with constant-volume gas thermometry, Guildner and Edsinger (1976) built an apparatus intended to study thermomolecular pressure differences. Their apparatus was comprised of concentric tubes with internal diameters of 0.8 mm and 9.8 mm. The tubes were connected to a differential pressure gauge at room temperature and they were connected to each other at the temperature to be studied. This approach of using two pressure-transmitting tubes for directly measuring the pressure difference could be adapted to RIGT to demonstrate *in situ* that the thermomolecular pressure differences were under control.

It is much easier to maintain a pressure constant with ppm resolution than it is to know the value of the same pressure with ppm uncertainty traceable to the SI. The RIGT requirement for SI-traceable, low-uncertainty pressure measurements is relaxed in the relative primary SPRIGT proposal of Gao *et al* (2017), prescribing measurements on single isobars (rather than isotherms) relative to a reference temperature. However, care must be taken to appropriately account for possible temperature-dependent effects along a given isobar. As such, the potential of the SPRIGT approach is strongest for temperatures below 25 K, because there density of helium gas is at least 10 times greater than at room temperature, the vapour pressures of many chemical contaminants are negligibly small, and the resonator compressibility κ_{eff} is nearly temperature-independent, so that compressibility effects are nearly cancelled out by the effect of the mathematical ratio

Table 2. Absolute primary microwave RIGT uncertainty budget from Rourke (2017), using helium as the working gas. All uncertainty components are listed as standard uncertainties.

	Triple point of neon $T_{90} = 24.5561$ K (mK)	Triple point of oxygen $T_{90} = 54.3584$ K (mK)	Triple point of argon $T_{90} = 83.8058$ K (mK)
T uncertainty components, Type B			
κ_{eff}	0.21	1.1	2.5
p calibration	0.19	0.4	0.7
p offset drift	0.20	0.2	0.6
p static head	0.15	0.2	0.2
Gas impurities	0.01	0.2	0.7
R literature	0.01	0.03	0.05
B_{ε} literature	0.18	0.2	0.2
B_{ρ} literature	0.13	0.06	0.05
Analysis model—direct p,T state evaluation compared with extrapolation to ideal gas limit	0.17	0.3	0.5
T uncertainty components, Type A			
p stability	0.13	0.02	0.03
$f_m(0)$ measurement and corrections	0.006	0.09	0.3
$f_m(p)$ measurement and half-width correction	0.01	0.07	0.2
Other $f_m(p)$ corrections	0.01	0.09	0.2
T combined standard uncertainty			
	0.49	1.3	2.8
T_{90} uncertainty components, Type B			
ITS-90 fixed point realization	0.2	0.2	0.2
CSPRT self-heating	0.1	0.1	0.1
Microwave heating	0.05	0.01	0.006
T_{90} combined standard uncertainty			
	0.23	0.22	0.22
$(T - T_{90})$ additional uncertainty components, Type A			
Cryostat thermal gradient correction	0.01	0.02	0.2
Consistency between multiple microwave modes	0.03	0.07	0.3
Consistency between points at different pressures on multiple isotherms	0.15	0.2	0.6
$(T - T_{90})$ combined standard uncertainty			
	0.56	1.3	2.9

at constant pressure. The thermal expansion coefficient and temperature dependence of the electrical conductivity of the resonator shell are also reduced at low temperatures. Some advantages of SPRIGT compared with other variants of RIGT are a short measurement time (time-consuming pressure extrapolations are not used) and reduced demands on the mechanical stability of the resonator due to the stable pressure environment throughout the experiment. Disadvantages of SPRIGT include the need for a reference temperature, the absence of redundant data from multiple measuring pressures, and the requirement for careful design of the cryostat gas line tubing in order to allow low uncertainty estimation of the hydrostatic head correction at each temperature. The SPRIGT apparatus is comprised mainly of three sub-systems, namely the cryostat system cooled using a two-stage pulse-tube (Gao *et al* 2018, Chen *et al* 2019), the gas-handling system where pressure is maintained constant by a servo-loop (Han *et al* 2018) and the microwave system at the heart of which lies the quasi-spherical resonator (Zhang *et al* 2019).

7. Uncertainty budgets

In order to illustrate the combined effects on RIGT experiments of the topics discussed in the preceding sections, uncertainty budgets are given for three very different RIGT approaches: absolute primary microwave RIGT, relative primary microwave SPRIGT, and absolute primary optical RIGT.

An uncertainty budget for absolute primary microwave RIGT measurements comparing the thermodynamic temperature T to the International Temperature Scale of 1990 (ITS-90) temperature T_{90}, using helium as the working gas, is shown in table 2. This table has been adapted from Rourke (2017), and omits uncertainty components that are less than or equal to 20 µK at all three measurement temperatures: Type B contributions to the uncertainty in T from literature values of the virial coefficients A_{ε}, A_{μ}, C_{ε}, C_{ρ} and D_{ρ}; and Type B contributions to the uncertainty in T_{90} from realization of the triple point of water, resistance bridge ratio measurements and standard resistor stability. While not explicitly discussed

in Rourke (2017), a Type B uncertainty component due to the uncorrected thermomolecular pressure effect would also fall into this category. This uncertainty budget applies to the main 'direct (p, T) state evaluation' analysis of Rourke (2017) described in section 2 above, with the results of the 'ideal gas extrapolation' analysis included in the form of the 'analysis model' uncertainty component.

At $T_{90} = 24.5561$ K, table 2 includes many uncertainty components of similar size, each approximately 0.2 mK. The uncertainty contribution due to resonator compressibility, κ_{eff}, comes mainly from a 2 GPa uncertainty in the literature value of the adiabatic bulk modulus of OFHC copper. The influence of this uncertainty on T scales as T^2, dominating the uncertainty budget at higher temperatures. A pressure balance was not used for pressure control during isotherm measurements, but rather was employed to calibrate a separate pressure transducer; the 'p offset drift' component corresponds to the uncertainty in the correction of the zero drift of this transducer between calibrations. As described in section 6, the static pressure head correction is larger at lower temperatures, amounting to 49(6) μPa Pa^{-1} (49(6) ppm) at 24.5561 K, 25(4) μPa Pa^{-1} (25(4) ppm) at 54.3584 K and 15(2.5) μPa Pa^{-1} (15(2.5) ppm) at 83.8058 K. The effects of decreased impurity vapour pressures at low temperatures mentioned in section 6 are also visible in table 2: xenon impurities did not contribute below 83.8058 K, and at 24.5561 K the only non-filtered gas impurity species with significant vapour pressure was neon. No uncertainty component for temperature stability was included, because the effects of thermal fluctuations on T and T_{90} are correlated and cancel out of the difference $T - T_{90}$; poorer thermal stability at 24.5561 K did, however, degrade pressure stability and therefore increased the uncertainty contribution from that component. For additional details and further discussion about individual uncertainty components, see Rourke (2017).

Planned experimental upgrades are foreseen to improve future uncertainty budgets relative to that of Rourke (2017) in several key areas. As described in section 5, *in situ* microwave measurements of resonator compressibility at the temperature of the triple point of water can reduce the uncertainty in κ_{eff}. As discussed in sections 3–6, a further reduction in the size of the uncertainty component on T due to κ_{eff}, along with the components due to gas impurities, $f_m(0)$, and $f_m(p)$, can be gained by using neon or argon instead of helium. Finally, cryostat and gas-handling system refinements can allow uncertainty contributions due to cryostat thermal gradient correction and p offset drift to be eliminated, the uncertainty contribution due to p static head to be reduced, and isotherms to be extended to higher pressures.

A projected uncertainty budget for future T measurements using the relative primary microwave SPRIGT technique, with helium as the working gas, is shown in figure 2, adapted from Gao *et al* (2017). Since this is a relative, not absolute, primary RIGT implementation, all T measurements are determined with respect to a reference thermodynamic temperature T_{ref}, which is calculated from the literature value and uncertainty of $T - T_{90}$ at a chosen reference T_{90}. A significant advantage of relative SPRIGT is clearly visible in that uncertainty contributions due to absolute pressure measurement and resonator
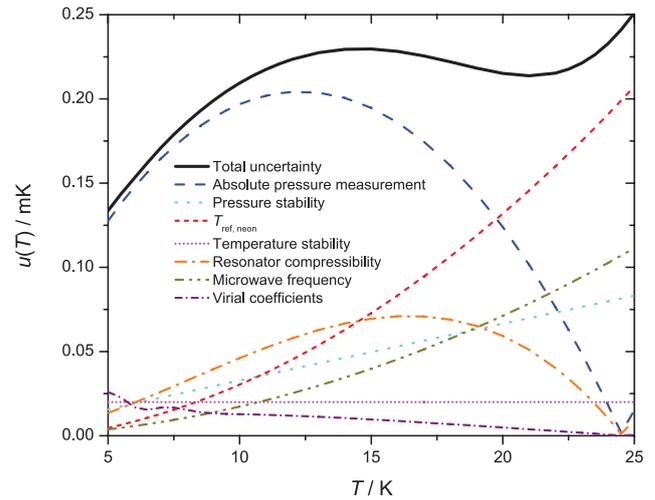
Figure 2. Projected uncertainty budget for future relative primary microwave RIGT measurements from Gao *et al* (2017). All uncertainty components are plotted as standard uncertainties.

compressibility go to zero at T_{ref} (in this case, the ITS-90 temperature of the triple point of neon, $T_{90} = 24.5561$ K, and the literature value of $T - T_{90}$ at that temperature is used to specify T_{ref}). However, below about 20 K, uncertainty in the absolute pressure measurement (which includes uncertainty in the static head correction) dominates the uncertainty budget. Above 20 K, the largest uncertainty contribution to T is due to the determination of T_{ref}, which includes the realization uncertainty of the ITS-90 neon fixed point and uncertainty in the literature value of ($T - T_{90}$) at $T_{90} = 24.5561$ K. For additional details and further discussion about individual uncertainty components, see Gao *et al* (2017).

An uncertainty budget for an absolute primary optical RIGT measurement of the Boltzmann constant at room temperature ($T = 293.1529$ K), using helium as the working gas, is shown in table 3. This table has been adapted from Egan *et al* (2017), and omits uncertainty components that are less than or equal to 0.05 μJ K^{-1}/(J K^{-1}) (0.05 ppm, equivalent to 15 μK at 293 K): uncertainties in the literature values of all virial coefficients higher than A_{R}, and uncertainty in the determination of the vacuum wavelength of the interferometer laser. For reader convenience, the relative uncertainties on the determination of the Boltzmann constant have also been converted into equivalent temperature uncertainties, though if Egan *et al* had analyzed their optical RIGT data to determine $T - T_{90}$ rather than the Boltzmann constant, their uncertainty contribution due to thermodynamic temperature T would be replaced by a smaller one due to T_{90}, and a new uncertainty component due to the uncertainty in the molar gas constant $R = N_{\text{A}}k$ would be added.

The optical RIGT uncertainty budget has a few notably different types of uncertainty component than the microwave RIGT uncertainty budgets. The dominant uncertainty contribution for microwave RIGT due to resonator compressibility is replaced by an uncertainty contribution arising from geometric thinning and stress-induced changes in the refractive index of the optical window, d_w, as pressure inside the optical cell increases. The multi-cell experimental arrangement

Table 3. Absolute primary optical RIGT uncertainty budget from a measurement of the Boltzmann constant k at $T = 293.1529\,\text{K}$ by Egan *et al* (2017), using helium as the working gas. All uncertainty components are listed as standard uncertainties.

Uncertainty component	$u_{\text{r}}(k) \times 10^6$	$u_{\text{r}}(k) \times 293.1529\,\text{K}$
Optical window distortion and stress, d_w	9.8	2.9 mK
Thermodynamic temperature, T	4.5	1.3 mK
Gas pressure, p	4.3	1.3 mK
Gas impurities	4.0	1.2 mK
Interferometric phase change, $\Delta\Phi$	2.2	0.64 mK
Relative cell length, ΔL	0.6	0.2 mK
Refractivity first virial coefficient, A_{R}	0.12	0.035 mK
k combined standard uncertainty	12.5	3.7 mK

of Egan *et al* (2017) allowed them to mostly cancel out the d_w term, though the residual uncertainty of this cancellation, largely due to beam incidence mismatch, still formed the largest component of their uncertainty budget. Uncertainty in the interferometric phase change, $\Delta\Phi$, combines subcomponents due to interferometer stability, periodic non-linearity, and phasemeter accuracy. The uncertainty in the difference between cell lengths, ΔL, includes contributions from coordinate-measuring machine measurement, surface form, silicate-bond thickness, end-face tilt and beam deviation. Planned refinements that are envisaged to improve future optical RIGT uncertainty budgets include improved beam alignment and next-generation cells made from low-thermal-expansion glass ceramic, with a reduction of d_w by a factor of three. For additional details and further discussion about individual uncertainty components, see Egan *et al* (2017).

8. Conclusions and prospects for future development

The principles and techniques of refractive-index gas thermometry are reviewed, with a focus on helium-based microwave RIGT using quasi-spherical resonators. In particular, considerations related to working gas thermophysical properties, purity and pressure measurement, refractive index measurement, and resonator compressibility are discussed in detail, and uncertainty budgets provided for three different RIGT approaches.

Considerable further progress in refining RIGT is expected, as on-going research in several areas matures. Given that the uncertainty in resonator compressibility is presently the largest component of absolute primary microwave RIGT realizations, improvements to the determination of this quantity, including extrapolation to low temperature of values measured at the triple point of water, offer the most direct target for reducing overall RIGT uncertainty budgets. Alternately, working gases such as neon or argon, which are less sensitive to uncertainties of the resonator's compressibility, gaseous impurities,

etc, should be further explored. Relative primary RIGT measurements on isobars, particularly at low temperatures where temperature dependence of resonator physical properties is reduced, may allow pressure measurement constraints to be relaxed compared to the levels required for absolute primary RIGT. Research to extend the use of microwave resonators to temperatures much higher than the triple point of water in support of AGT shows some promise, though considerable technical challenges relating to resonator compressibility, resonator stability, gas purity and gas density requirements remain to be resolved before RIGT becomes feasible in this temperature range; and these challenges are more severe for RIGT than for AGT at high temperatures. Finally, further development of optical RIGT should be pursued, since its techniques and sources of uncertainty differ significantly from those of microwave RIGT, allowing entirely different avenues for advancement.

Acknowledgments

References

Barter C, Meisenheimer R G and Stevenson D P 1960 Diamagnetic susceptibilities of simple hydrocarbons and volatile hydrides *J. Phys. Chem.* **64** 1312–6

Bich E, Hellmann R and Vogel E 2008 *Ab initio* potential energy curve for the neon atom pair and thermophysical properties for the dilute neon gas. II. Thermophysical properties for low-density neon *Mol. Phys.* **106** 1107–22

Bruch L W and Weinhold F 2000 Diamagnetism of helium *J. Chem. Phys.* **113** 8667–70

Bruch L W and Weinhold F 2002 Nuclear motion and Breit–Pauli corrections to the diamagnetism of atomic helium *J. Chem. Phys.* **117** 3243–7

Bruch L W and Weinhold F 2003 Nuclear motion and Breit–Pauli corrections to the diamagnetism of atomic helium *J. Chem. Phys.* **119** 638 (erratum)

Cencek W, Garberoglio G, Harvey A H, McLinden M O and Szalewicz K 2013 Three-body nonadditive potential for argon with estimated uncertainties and third virial coefficient *J. Phys. Chem.* A **117** 7542–52

Cencek W, Komasa J and Szalewicz K 2011 Collision-induced dipole polarizability of helium dimer from explicitly correlated calculations *J. Chem. Phys.* **135** 014301

Cencek W, Przybytek M, Komasa J, Mehl J B, Jeziorski B and Szalewicz K 2012 Effects of adiabatic, relativistic, and quantum electrodynamics interactions on the pair potential and thermophysical properties of helium *J. Chem. Phys.* **136** 224303

Chen Y *et al* 2019 Thermal response characteristics of a SPRIGT primary thermometry system *Cryogenics* **97** 1–6

Colclough A R 1974 A projected refractive index thermometer for the range 2–20 K *Metrologia* **10** 73–74

Cui J, Feng X J, Lin H, Zhang J T and Huan K W 2018 Thermodynamic temperature measurement using single cylindrical microwave resonator *Jiliang Xuebao/Acta Metrol. Sin.* **39** 255–61

de Podesta M, Sutton G, Underwood R, Bell S, Stevens M, Byrne T and Joseph-Franks P 2011 Outgassing of water vapour, and its significance in experiments to determine the Boltzmann constant *Metrologia* **48** L1–L6

Edwards G and Underwood R 2011 The electromagnetic fields of a triaxial ellipsoid calculated by modal superposition *Metrologia* **48** 114–22

Egan P F, Stone J A and Scherschligt J K 2019 Measured relationship between thermodynamic pressure and refractivity for six candidate gases in laser barometry submitted to *J. Vac. Sci. Technol.* A

Egan P F, Stone J A, Ricker J E and Hendricks J H 2016 Comparison measurements of low-pressure between a laser refractometer and ultrasonic manometer *Rev. Sci. Instrum.* **87** 053113

Egan P F, Stone J A, Ricker J E, Hendricks J H and Strouse G F 2017 Cell-based refractometer for pascal realization *Opt. Lett.* **42** 2944–7

Fellmuth B, Engert J, Shimazaki T and Sparasci F 2018 *Guide to the Realization of the ITS-90, Chapter 3: Vapour Pressure Scales and Pressure Measurements* (Sèvres: Bureau International des Poids et Mesures) 22p (1 January 2018) (https://bipm.org/en/committees/cc/cct/guide-its90.html) version

Feng X J, Gillis K A, Moldover M R and Mehl J B 2013 Microwave-cavity measurements for gas thermometry up to the copper point *Metrologia* **50** 219–26

Gaiser C and Fellmuth B 2016 Method for extrapolating the compressibility data of solids from room to lower temperatures *Phys. Status Solidi* b **253** 1549–56

Gaiser C and Fellmuth B 2018 Polarizability of helium, neon, and argon: new perspectives for gas metrology *Phys. Rev. Lett.* **120** 123203

Gaiser C and Fellmuth B 2019 Highly-accurate density-virial-coefficient values for helium, neon and argon at 0.01 °C determined by dielectric-constant gas thermometry *J. Chem. Phys.* **150** 134303

Gaiser C, Zandt T and Fellmuth B 2015 Dielectric-constant gas thermometry *Metrologia* **52** S217–26

Gao B *et al* 2018 Realization ultra-high precision temperature stabilization in the cryogen-free cryostat for the SPRIGT *Rev. Sci. Instrum.* **89** 104901

Gao B, Pitre L, Luo E C, Plimmer M D, Lin P, Zhang J T, Feng X J, Chen Y Y and Sparasci F 2017 Feasibility of primary thermometry using refractive index measurements at a single pressure *Measurement* **103** 258–62

Garberoglio G and Harvey AH 2011 Path-integral calculation of the third virial coefficient of quantum gases at low temperatures *J. Chem. Phys.* **134** 134106

Garberoglio G, Moldover M R and Harvey A H 2011 Improved first-principles calculation of the third virial coefficient of helium *J. Res. Natl Inst. Stand. Technol.* **116** 729–42

Gavioso R M *et al* 2011 Progress in INRiM experiment for the determination of the Boltzmann constant with a quasi-spherical resonator *Int. J. Thermophys.* **32** 1339–54

Gavioso R M, Madonna Ripa D, Steur P P M, Gaiser C, Truong D, Guianvarc'h C, Tarizzo P, Stuart F M and Dematteis R 2015 A determination of the molar gas constant *R* by acoustic thermometry in helium *Metrologia* **52** S274–304

Guildner L A and Edsinger R E 1976 Deviation of international practical temperatures from thermodynamic temperatures in the temperature range from 273.16 K to 730 K *J. Res. Natl Bur. Stand.* **80A** 703–38

Han D *et al* 2018 Ultra-stable pressure is realized for Chinese single pressure refractive index gas thermometry in the range 30–90 kPa *Sci. Bull.* **63** 1601–3

Hättig C, Cacheiro J L, Fernández B and Rizzo A 2003 *Ab initio* calculation of the refractivity and hyperpolarizability second virial coefficients of neon gas *Mol. Phys.* **101** 1983–95

Heller D F and Gelbart W M 1974 Short range electronic distortion and the density dependent dielectric function of simple gases *Chem. Phys. Lett.* **27** 359–64

Hernandez A, Martin E, Margineda J and Zamarro J M 1986 Resonant cavities for measuring the surface resistance of metals at X-band frequencies *J. Phys. E: Sci. Instrum.* **19** 222–5

Huot J and Bose T K 1991 Experimental determination of the dielectric virial coefficients of atomic gases as a function of temperature *J. Chem. Phys.* **95** 2683–7

Inagaki S, Ezura E, Liu J-F and Nakanishi H 1997 Thermal expansion and microwave surface reactance of copper from the normal to the anomalous skin effect region *J. Appl. Phys.* **82** 5401–10

Jäger B, Hellmann R, Bich E and Vogel E 2011 *Ab initio* virial equation of state for argon using a new nonadditive three-body potential *J. Chem. Phys.* **135** 084308

Janney D H 1957 Accuracy of a microwave resonant cavity measurement of the velocity of light *Phys. Rev.* **105** 1138–40

Jousten K *et al* 2017 Perspectives for a new realization of the pascal by optical methods *Metrologia* **54** S146–61

Levy M and Perdew J P 1985 Hellmann–Feynman, virial, and scaling requisites for the exact universal density functionals. Shape of the correlation potential and diamagnetic susceptibility for atoms *Phys. Rev.* A **32** 2010–21

May E F, Pitre L, Mehl J B, Moldover M R and Schmidt J W 2004 Quasi-spherical cavity resonators for metrology based on the relative dielectric permittivity of gases *Rev. Sci. Instrum.* **75** 3307–17

Mehl J B 2009 Second-order electromagnetic eigenfrequencies of a triaxial ellipsoid *Metrologia* **46** 554–59

Mehl J B 2015 Second-order electromagnetic eigenfrequencies of a triaxial ellipsoid II *Metrologia* **52** S227–32

Mehl J B, Moldover M R and Pitre L 2004 Designing quasi-spherical resonators for acoustic thermometry *Metrologia* **41** 295–304

Migliori A and Sarrao J 1997 *Resonant Ultrasound Spectroscopy* (New York: Wiley) 201p

Moldover M R, Gavioso R M, Mehl J B, Pitre L, de Podesta M and Zhang J T 2014 Acoustic gas thermometry *Metrologia* **51** R1–19

Moldover M R, Schmidt J W, Gillis K A, Mehl J B and Wright J D 2015 Microwave determination of the volume of a pressure vessel *Meas. Sci. Technol.* **26** 015304

Moszynski R, Heijmen T G A and van der Avoird A 1995 Second dielectric virial coefficient of helium gas: quantum-statistical calculations from an *ab initio* interaction-induced polarizability *Chem. Phys. Lett.* **247** 440–6

Pavese F and Molinar Min Beciet G 2013 *Modern Gas-Based Temperature and Pressure Measurements* (New York: Springer) 650p

Pitre L, Moldover M R and Tew W L 2006 Acoustic thermometry: new results from 273 K to 77 K and progress towards 4 K *Metrologia* **43** 142–62

Pitre L, Sparasci F, Truong D, Guillou A, Risegari L and Himbert M E 2011 Measurement of the Boltzmann constant k_B using a quasi-spherical acoustic resonator *Int. J. Thermophys.* **32** 1825–86

Podobedov B 2009 Resistive wall wakefields in the extreme anomalous skin effect regime *Phys. Rev. ST Accel. Beams* **12** 044401

Puchalski M, Piszczatowski K, Komasa J, Jeziorski B and Szalewicz K 2016 Theoretical determination of the polarizability dispersion and the refractive index of helium *Phys. Rev.* A **93** 032515

Rizzo A, Hättig C, Fernández B and Koch H 2002 The effect of intermolecular interactions on the electric properties of helium and argon. III. Quantum statistical calculations of the dielectric second virial coefficients *J. Chem. Phys.* **117** 2609–18

Rourke P M C 2017 NRC microwave refractive index gas thermometry implementation between 24.5 K and 84 K *Int. J. Thermophys.* **38** 107

Rourke P M C and Hill K D 2015 Progress toward development of low-temperature microwave refractive index gas thermometry at NRC *Int. J. Thermophys.* **36** 205–28

Rusby R L 1975 Proposal for dielectric-constant (or refractive-index) gas thermometry in the range 90–373 K *Inst. Phys. Conf. Ser. for Eur. Conf. on Temp. Meas.* vol 26 pp 44–8

Ruud K, Skaane H, Helgaker T, Bak K L and Jørgensen P 1994 Magnetizability of hydrocarbons *J. Am. Chem. Soc.* **116** 10135–40

Schmidt J W, Gavioso R M, May E F and Moldover M R 2007 Polarizability of helium and gas metrology *Phys. Rev. Lett.* **98** 254504

Shaul K R S, Schultz A J and Kofke D A 2012 Path-integral Mayer-sampling calculations of the quantum Boltzmann contribution to virial coefficients of helium-4 *J. Chem. Phys.* **137** 184101

Simon N J, Drexler E S and Reed R P 1992 *Properties of Copper and Copper Alloys at Cryogenic Temperatures* (*National Institute Standards Technology Monograph* vol 177) (Washington, DC: U.S. Government Printing Office) pp 1–850

Steur P P M, Fellmuth B and Tamura O 2018 *Guide to the Realization of the ITS-90, Chapter 4: Interpolating Constant-Volume Gas Thermometry* (Sèvres: Bureau International des Poids et Mesures) 16p (1 January 2018) (https://bipm.org/en/committees/cc/cct/guide-its90.html) (version)

Tischer F J 1976 Excess conduction losses at millimeter wavelengths *IEEE Trans. Microw. Theory Technol.* **24** 853–8

Underwood R J and Edwards G J 2014 Microwave-dimensional measurements of cylindrical resonators for primary acoustic thermometry *Int. J. Thermophys.* **35** 971–84

Underwood R J, Mehl J B, Pitre L, Edwards G, Sutton G and de Podesta M 2010 Waveguide effects on quasispherical microwave cavity resonators *Meas. Sci. Technol.* **21** 075103

Underwood R, de Podesta M, Sutton G, Stanger L, Rusby R, Harris P, Morantz P and Machin G 2016 Estimates of the difference between thermodynamic temperature and the international temperature scale of 1990 in the range 118 K to 303 K *Phil. Trans. R. Soc.* A **374** 20150048

Underwood R, Flack D, Morantz P, Sutton G, Shore P and de Podesta M 2011 Dimensional characterization of a quasispherical resonator by microwave and coordinate measurement techniques *Metrologia* **48** 1–15

Vogel E, Jäger B, Hellmann R and Bich E 2010 *Ab initio* pair potential energy curve for the argon atom pair and thermophysical properties for the dilute argon gas. II. Thermophysical properties for low-density argon *Mol. Phys.* **108** 3335–52

Wiebke J, Pahl E and Schwerdtfeger P 2012 Up to fourth virial coefficients from simple and efficient internal-coordinate sampling: application to neon *J. Chem. Phys.* **137** 014508

Wiebke J, Schwerdtfeger P, Moyano G E and Pahl E 2011 An atomistic fourth-order virial equation of state for argon from first principles calculations *Chem. Phys. Lett.* **514** 164–7

Yang I, Underwood R and de Podesta M 2018 Investigating the adequacy of a low-cost vector network analyser for microwave measurements in quasispherical resonators *Meas. Sci. Technol.* **29** 075013

Yoshizawa T and Hada M 2009 Relativistic and electron-correlation effects on magnetizabilities investigated by the Douglas–Kroll–Hess method and the second-order møller-plesset perturbation theory *J. Comput. Chem.* **30** 2550–66

Zandt T, Sabuga W, Gaiser C and Fellmuth B 2015 Measurement of pressures up to 7 MPa applying pressure balances for dielectric-constant gas thermometry *Metrologia* **52** S305–13

Zhang H Y *et al* 2019 A high-stability quasi-spherical resonator in SPRIGT for microwave frequency measurement at low temperatures *Sci. Bull.* **64** 286–8

Zhang K, Feng X J, Gillis K, Moldover M, Zhang J T, Lin H, Qu J F and Duan Y N 2016 Acoustic and microwave tests in a cylindrical cavity for acoustic gas thermometry at high temperature *Phil. Trans. R. Soc.* A **374** 20150049

Zhang K, Feng X J, Zhang J T, Lin H, Duan Y N and Duan Y Y 2017 Microwave measurements of the length and thermal expansion of a cylindrical resonator for primary acoustic gas thermometry *Meas. Sci. Technol.* **28** 015006